Mobile Microgrid for Energy Resiliency

EPRI GridEd Undergraduate Design Final Report for project PO Number 4700007562

Dylan Miley (dcmiley@iastate.edu) and Abdelrahman Mannan (ammannan@iastate.edu)

1. Abstract

An undergraduate senior design electrical engineering team (2020-2021 academic year) proposed 1) to simulate a microgrid design for a load to be powered during an emergency and to analyze the economics of this design, and 2) to design, build and test a working small scale offgrid nanogrid, focusing on electrolysis (hydrogen production) and power generation from a hydrogen fuel cell. The project developed from a working demonstration mobile microgrid at ISU, developed for disaster response. The objective of this work is to simulate microgrid operations for economic viability and to build a working hydrogen energy nanogrid.

2. Microgrid simulation for energy adequacy and performance evaluation

The team developed a 25-year energy adequacy model (EAM) to evaluate performance using MATLAB and real data for solar irradiance (NREL NSRDB (National Solar Resource Database), temperature, and load shape for an Iowa care facility. The simulation used an electrical model of a PV array, a state-of-charge model for a Li+ phosphate battery, and an energy management system. The size was optimized by HOMER to meet the load demand for the lowest Levelized Cost of Energy (LCOE). The model outputs power produced by solar, load demand met by solar energy, spilled solar energy, state of charge of the battery, load demand met by the battery, and percent of the load demand that is met/unmet. A Levelized Cost of Energy (LCOE) of 0.53 [$/kWh] was calculated with the energy production data.

The average daily energy consumption for the health care facility was 309.67 kWh and the peak power requirement was 28.6 kW. The results of the HOMER analysis gave a battery capacity of 944 kWh and solar PV panel sized at 176 kW to sustain the load. When energy produced by PV is insufficient to meet the load, the battery discharges; When there is excess energy, the battery charges. Excess PV is quantified as spilled PV and is indicative of overdesign for the application. The HOMER optimized microgrid design was implemented in the EAM and the results of the analysis are shown in Figure 1.

Tracing the energy flow throughout the system indicates how the system is responding to the load demanded, where the solar-generated power is going, and whether production exceeds demand. Figure 1 shows for each hour of year 1, a) the estimated amount of PV power produced in units of kW, b) load (kW), c) Stored energy (kW*h*) and d) the difference between PV to the load and PV to the battery (spilled energy). This figure indicates where the energy produced PV array is going, i.e stored in the battery or spilled when it exceeds the battery's capacity.

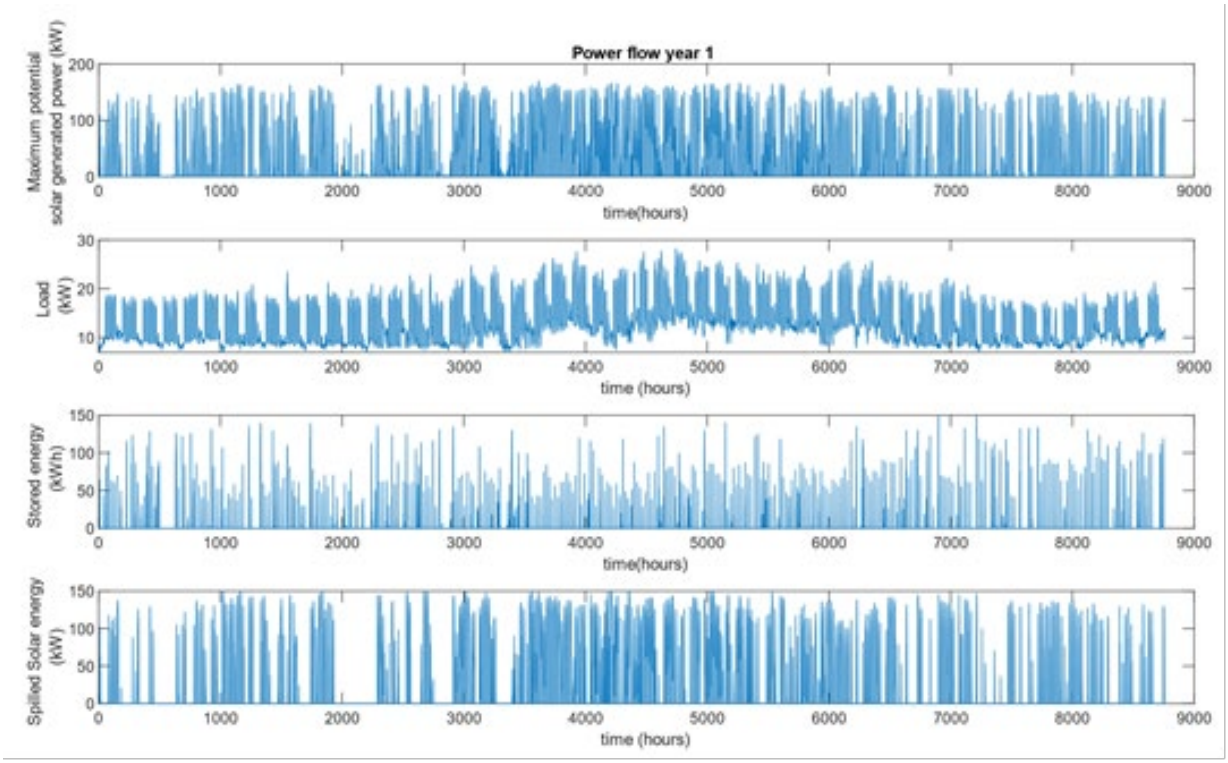

Figure 1. Power flow trace for year 1

In hour 10 the PV array production is greater than the load, and since the battery is at 100% SOC the solar PV array feeds the load and the remainder is considered spilled power. Although the primary objective of the system is to power the load, there are instances where the load is not met. Starting in hour 10, for example, there are consecutive periods of insufficient irradiance levels, which in turn leads to insufficient solar power being generated, hence the battery gets depleted for an extended period of time. In subsequent years, the PV panels and the battery experience degradation (PV degradation assumed to be 0.7% per year, battery degradation assumed to be 8% per year). As a result the system's ability to sustain the load likewise decreases, so the percentage of unmet demand increases. The solar degradation has a compounding effect on unmet demand: as the project progress the % of unmet load increases exponentially. In our model, degradation of the solar PV array influences how the whole system behaves and whether it can sustain the load. Knowing the rate of degradation informs timing for replacements. NREL (2020) compared PV degradation factors: "78% of all systems reported a decrease in efficiency rate of less than 1%/year, with a degradation of 3% in the first year of usage and 0.7%/year every following year" [3]. The battery also degrades over time. The battery's lifetime is measured by the number of charging/discharging cycles. Every full charging/discharging cycle corresponds to some loss of the battery's performance. Most Li-Ion batteries lose roughly 0.025%-0.048% of their capacity per cycle [4]. The number of charge cycles was calculated by analyzing the SOC trend for each year and using a simple rainfall counting algorithm to count the charging/discharging instances. The SOC plot was inverted, and each valley/peak corresponds to a fraction of a complete charge/discharge cycle. The charge/discharge cycles were accumulated and then carried over to the next year including the losses associated with each cycle [5][6]. Each complete charge cycle corresponds to some level of degradation in the battery. As the project progresses, with degradation of the PV array, the reliance on the battery increases resulting in increasing degradation.

Microgrid costs were extrapolated from actual costs of the ISU mobile microgrid. The economic analysis was based on 2020 costs for a PV-battery mobile microgrid system developed by ISU with funding from the Iowa Economic Development Authority [7]. To calculate the LCOE, we assumed all energy used to feed the load came from PV directly, or was first stored in the battery and released on demand. The LCOSS (Levelized Cost Of Solar and Storage) outlined in [8] is an extension of the LCOE. It considers both the PV array and BESS (Battery Energy Storage System) as entities capable of feeding the load. In addition, it includes variables associated with the running cost of the project like follow on/replacement investment at a given year. Tax rate, depreciation, and debt payments were omitted for this case study.

$$LCOSS = \frac{I + \sum_{t=1}^{n} \frac{O\&M_t}{(1+d)^t} + \frac{F_t}{(1+d)^t}}{\sum_{t=1}^{n} \frac{E_0(1-\alpha)^t}{(1+d)^t}(1-B) + \sum_{t=1}^{n} \frac{E_0(1-\alpha)^t}{(1+d)^t} B(1-\gamma)^t} \qquad (1)$$

$E_0 = Annual\ Energy\ produced$: 293500kWh
$\alpha = PV\ degradation\ Factor$ [%], PV cells assumed to degrade 3% in year 1, then 0.7% each year
$n = duration\ of\ project$ $[years]$, 25 years
$t = current\ year$ $[years]$
$d = discount\ factor$ [%], 5.3%, current US inflation rate
$I = Initial\ Investment$ [$] $1,128,742
$O\&M = Fixed\ Operation\ \&$ Maintenance $23,239
$F = Follow\ on\ Investment\ at\ year\ t$ [$] $485,312 in year 10
$B = Energy$ generated from [%] 18%
$\gamma = Battery\ degradation$ (8%), battery and PV array replaced at 80% capacity

The EAM was developed to help address some of the questions that arise in the planning phase of a microgrid project. With considerations for component degradation and system losses, the EAM tool provides a realistic way to analyze the system's performance for long term planning. In addition, the economic analysis provides a benchmark for comparison with alternatives. The primary objective of the HOMER analysis is to optimize the tradeoff between minimizing the amount of demand not met, and the price of the system. Coupling our system with the HOMER analysis provides more flexibility by allowing the user to investigate how much of the met load they may be willing to give up to reduce the cost. For solar and wind resources affected by climate zone, oversizing the system will still not provide enough power because the weather does not permit. In general, the EAM tool is intended to expand on the preexisting optimization capabilities of HOMER and allow room for more decisions. The EAM tool grants the system designer the ability to relax some of the constraints such as such as continuously sustaining the load, thus, enabling a broader range of design objectives to be achieved.

3. EPRC Nanogrid

3.1 Nanogrid: an overview

The nanogrid was designed to be self-contained with a point of common coupling. In this way, the nanogrid is quite similar to a microgrid, but on a Watt scale. The ISU EPRC team designed and assembled a portable nanogrid with the following primary components: solar panel (100W), battery (518Wh), hydrogen (H_2) electrolyzer (18W), hydrogen purification system, and H_2 fuel cell (30W). Each component of the EPRC Nanogrid is housed within a modified handcart with 2 shelves and a central mounting board. The battery is at the bottom of the handcart, a three-stage drying system is mounted on the back of the handcart, and the electrolyzer is mounted at the top of the handcart. The solar panel can be mounted on the back of the cart below the three-stage drier. In total the EPRC Nanogrid is 0.2 m^3 in size. Several pictures of the EPRC are displayed in. This nanogrid serves as a scale sized proof of concept to explore the functionality and performance of a closed-loop renewable energy system that generates, stores, and uses hydrogen for the purpose of supplying electrical energy.

3.2 From sun power to chemical energy

A small solar panel and battery were interfaced with each other and integrated into the nanogrid to serve as the baseline source of power. The solar panel is meant to supply the majority of the load when the sun is shining and will transfer any extra power produced to the battery. The battery serves as an energy source to bolster the solar panel, supply power when the sun has set, and also can power the electrolyzer when hydrogen production is desired. Testing was performed on the solar panel and battery system to assure that the devices worked and to find what level of power can be produced during different weather conditions in Ames, Iowa. These results were standard and are excluded from this report, as the main point of interest is the hydrogen system.

3.3 H_2 as an energy carrier: a closed loop system

The H_2 subsystem of the EPRC Nanogrid is closed loop in the sense that H_2 electrolysis is powered by the nanogrid, the H_2 can then be used to supply a fuel cell that converts the H_2 to H_2O and electricity. In this way, the nanogrid stores generates and stores energy in the form of H_2 through use of electrolysis and the energy can be accessed through the use of a fuel cell. H_2 generated by the electrolyzer is inevitably mixed with water due to the nature of the polymer electrolyte membrane electrolyzer used. Moisture is removed from the H_2 with a three-step purification system. After purification, H_2 can be transferred into a storage tank or directly used by the fuel cell.

4. Experimental setup and testing procedures

4.1 The H_2 subsystem

The hydrogen system design evolved over several months. The system was built using commonly available National Pipe Thread standards (generally sized to ¼”NPT). Interconnections were sealed using Teflon tape rated for use with hydrogen. The maximum pressure produced by the electrolyzer is 145 PSI and all other components were selected to have a pressure rating of at least 225 PSI. The final design implements a series of valves to allow control over H_2 flow within the system. The valves can be opened or closed in 4 main combinations to direct H_2 flow within the system. No adaptations beyond valve operation are necessary for operation. The various H_2 flow possibilities and corresponding valve configurations are as follows: H_2 from electrolysis is sent to the storage tank (V1 open, V2 open, V3 closed), H_2 from electrolysis supplies the HFC (V1 open, V2 closed, V3 open), H_2 from the storage tank supplies the HFC (V1 closed, V2 open, V3 open), and H_2 from both the tank and electrolysis supply the HFC (V1 open, V2 open, V3 open). All aspects of the system can be vented independently or jointly through a central venting valve (V4).

Tests were performed throughout the stages of assembly of the H_2 system to assure that each component worked independently, and as part of the system. The electrolyzer was first tested to determine the amount of power needed and the amount of hydrogen that could be produced. Extensive testing was done on the piping system that transports the H_2 through the nanogrid, to eliminate leaks. During this testing, it was determined that several Schrader valve outputs didn’t work for our system, so we replaced the H_2 output fitting with a secure CGA fitting.

Preliminary HFC testing was performed with a proton-exchange membrane (PEM) fuel cell test bed that allowed for the investigation of power output as a function of H_2 humidity and temperature. The HFC power output was tested both with the nanogrid- generated hydrogen and with separately purchased, industry-grade H_2. The power generated by the fuel cell should not vary with hydrogen source, as the composition of either hydrogen gas has a near ~100% purity. The nanogrid was purged with H_2 prior to tests to reduce potential atmospheric contaminants in the system. After purging, either hydrogen source was passed through the three-stage purifier and into the fuel cell through a pressure regulator to

step the pressure down to the working pressure of the HFC (the HFC does not operate if the pressure and flow rate of H_2 is too low, and will purge excess H_2 if the pressure surpasses the working pressure of the cell). High pressures were avoided to reduce any potential damage to the cell membranes and to reduce wasted H_2. All tests were performed in a controlled lab setting in the lab of Dr. Wenzhen Li at the Iowa State Bio Renewables Laboratory.

5. Results

5.1 Hydrogen production through electrolysis

The electrolyzer required more power than the rated 18 W and on average required 27 W to operate at the rated 9 A. The pressure of H_2 produced increased throughout the duration of the test linearly by ~1 PSI per minute. Oversaturation of the electrolyzer with water resulted in excess water exiting the electrolyzer through the O2 and H_2 output ports. The water was removed with the three-stage drying system. A H_2 and H_2O separation chamber was used in the initial iterations but was later removed due to the excessive volume and redundance with the three-stage purifier. The hydrogen gas will pass through the liquid water and leave a majority of the water behind. The flow rate of produced hydrogen was not measured. Electrolysis was only performed until a maximum of 55 PSI system pressure was achieved. Further tests are required to determine the true limits of this system and to optimize the power generation and energy storage process.

5.2 Power production through H_2 separation

The HFC was first tested with H_2 from electrolysis. This H_2 was stored in the secondary storage tank as well as within the gas lines of the nanogrid. Prior to testing, the system was pressurized to 55 PSI. A programmable load was used to draw power from the HFC. The HFC was operated first in open circuit conditions and the constant power demand from the load was gradually increased in increments of 2 W. The changes in voltage and current took roughly 15 s to saturate with each increment. Any increase in power greater than 2 W led to the HFC operating in short circuit conditions. With each increment of power, the HFC voltage decreased and the current increased. The total H_2 supply was depleted shortly after the demanded power was increased to 20 W. Additionally, the depleting H_2 source resulted in a varying outlet pressure and inconsistency in fuel cell operation.

The HFC was then tested with the purchased H_2. The fuel cell behaved similarly in terms of time to saturate and exchange of voltage for current as the load on the HFC increased. The performance differed in that the supply of industrial H_2 was abundant, whereas the amount of electrolysis H_2 was relatively small. The abundance of industrial H_2 resulted in higher consistency of HFC operations, as the outlet pressure never varied. Within these tests, the HFC was able to handle larger steps of increase in power demanded by the load. The results of the HFC tests are depicted in the figure below, which represents the power, voltage and current characteristics of the most recent HFC test.

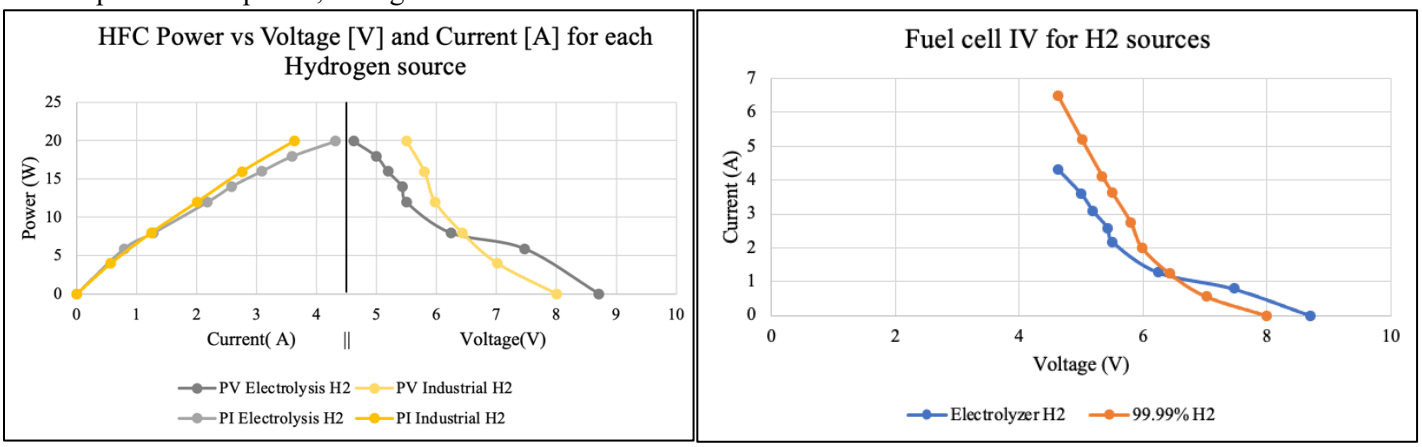

Figure 2: HFC power characteristics for differing H_2 sources

6.3 Discussion

The pressure of the outlet H_2 was not highly controlled due to the pressure requirements of the regulator used. The regulator was designed for stepping high pressure regimes surpassing 1000 PSI down to 0-150 PSI. This resulted in inaccurate indications of the outlet pressure of the system into the HFC. A pressure regulator designed for low pressure regimes would allow for direct knowledge of outlet pressure and increase the consistency of fuel cell operation. The performance of the HFC is directly dependent on the pressure and volume of the incoming H_2. Deviations in the H_2 supply alter the HFC power characteristics. For this reason, pressure deviation is a likely cause for the shift in behavior of the

HFC PV curve described in section 4.3. While the HFC was able to meet the power demanded from the device, the IV characteristics indicate a need for improvements to the system and further testing to optimize HFC performance.

The electrolyzer is not rated to produce 60mL/min until the maximum working pressure of 10 atm is reached. For this reason, the nanogrid is most efficient when the hydrogen system is kept at a maximum pressure. Electrolysis was only performed until a maximum of 55 PSI system pressure was achieved. This resulted in a scarce amount of H_2 that disallowed a test of the full operation of the electrolyzer. Further tests are needed to determine the true limits of this system and to optimize power generation and energy storage. An additional approach to improve the nanogrid performance is to decrease the volume of the system until the maximum working pressure of the electrolyzer is reached. Once the pressure approaches 145 PSI, a pressure regulator can be used to send hydrogen to the storage tank starting at low pressure and gradually increasing. This way, the electrolyzer remains in high pressure regimes and can output near the maximum flow rate of 60 mL/min.

7. Conclusion

The work summarized in this report encompasses both theoretical and experimental microgrid research. A simulation tool was developed for microgrid operations analysis that considers geographical weather characteristics and also load requirements. An economic viability analysis informed by the data yielded by this tool yielded an LCOSS of 0.533 $/kWh. Beyond simulation, a portable nanogrid was designed, developed, and tested. The nanogrid integrates solar energy production, battery storage, and hydrogen energy power conversion processes. The HFC was capable of supplying the power demanded by the load with both nanogrid generated and industrial H_2, however the voltage characteristics differed. The test results indicate areas in which the hydrogen system can be further improved, such as the outlet pressure regulation and procedure of hydrogen electrolysis. Further tests are also required to determine the hydrogen purity and respective HFC power characteristics.

8. Works Cited

[1] T. R. Teregulov, B. Sharifov and A. R. Valeev, "Simplified solar panel modeling in MATLAB/Simulink considering Bashkortostan Republic (Russia) environment characteristics," *2016 2nd International Conference on Industrial Engineering, Applications and Manufacturing (ICIEAM)*, 2016, pp. 1-4, doi: 10.1109/ICIEAM.2016.7911448.

[2] Y. Jiang, J. A. A. Qahouq and I. Batarseh, "Improved solar PV cell Matlab simulation model and comparison," *2010 IEEE International Symposium on Circuits and Systems (ISCAS)*, 2010, pp. 2770-2773, doi: 10.1109/ISCAS.2010.5537014.

[3] Jordan, D.C.; Kurtz, S.R. Photovoltaic degradation rates—An Analytical Review. Prog. Photovolt. Res. Appl. 2013, 21, 12–29.

[4] Spotnitz, R. Simulation of Capacity Fade in Lithium-Ion Batteries. J. Power Sources 2003, 113, 72–80.

[5] S.D. Downing, D.F. Socie, Simple rainflow counting algorithms, Int. J. Fatigue 4 (1) (1982) 31–40

[6] M. J. E. Alam and T. K. Saha, "Cycle-life degradation assessment of Battery Energy Storage Systems caused by solar PV variability," *2016 IEEE Power and Energy Society General Meeting (PESGM)*, 2016

[7] Final Report to Iowa Economic Development Authority. Mobile Energy Storage for Resiliency. Anne Kimber (akimber@iastate.edu)

[8] Ramasamy Vignesh, David Feldman, Jal Desai, and Robert Margolis. 2021. U.S. Solar Photovoltaic System and Energy Storage Cost Benchmarks: Q1 2021. Golden, CO: National Renewable Energy Laboratory. NREL/TP-7A40-80694.

[9] STANDARD FOR HYDROGEN PIPING SYSTEMS AT USER LOCATIONS AIGA 087/14

[10] 8-2012 Optimal Energy Management for Microgrids Zheng Zhao,Clemson University

[11] F. Serra, M. Petrollese, M. Lucariello and G. Cau, "Assessment of a hydrogen production, storage and utilization system in a demonstrative microgrid," *2020 2nd IEEE International Conference on Industrial Electronics for Sustainable Energy Systems (IESES)*, 2020, pp. 157-162, doi: 10.1109/IESES45645.2020.9210669